Preferred citation: P.J. Krochak, J.A. Olson and D.M. Martinez. Near-wall estimates of the concentration and orientation distribution of semi-dilute rigid fiber suspensions in Poisieulle flow. In **Advances in Pulp and Paper Research, Oxford 2009**, *Trans. of the XIVth Fund. Res. Symp. Oxford, 2009*, (S.J. I'Anson, ed.), pp 181–206, FRC, Manchester, 2018. DOI: 10.15376/frc.2009.1.181.

NEAR-WALL ESTIMATES OF THE CONCENTRATION AND ORIENTATION DISTRIBUTION OF SEMI-DILUTE RIGID FIBER SUSPENSIONS IN POISIEULLE FLOW

Paul J. Krochak[1], James A. Olson[2] and D. Mark Martinez[3]

[1]The Pulp and Paper Center, Dept. of Mechanical Engineering
The University of British Columbia, 2324 Main Mall, Vancouver BC, V6T 1Z4, Canada
[2]The Pulp and Paper Center, Dept. of Mechanical Engineering
The University of British Columbia, 2324 Main Mall, Vancouver BC, V6T 1Z4, Canada
[3]Dept. of Chemical and Biological Engineering,
The University of British Columbia, 2360 East Mall, Vancouver, BC, V6T 1Z3, Canada

ABSTRACT

A model is presented to describe the orientation and concentration state of semi-dilute, rigid fiber suspensions in a rectangular channel flow. A probability distribution function is used to describe the local orientation and concentration state of the suspension and evolves according to a Fokker-Plank type equation. Long range hydrodynamic fiber-fiber interactions are modeled using the approach outlined by Folgar and Tucker (*J. Reinforced Plast. Comp.* **3** 98–119 1984). Near the channel walls, we apply the no-flux boundary conditions proposed

by Schiek and Shaqfeh (*J. Fluid Mech.* **296**, 271–324, 1995). Geometric constraints are used to couple the fibers' rotary motion with its translational motion. This eliminates physically unrealistic orientation states in the near-wall region. A two-way coupling between the fiber orientation state and the momentum equations of the suspending fluid is considered. Experiments are performed to validate the numerical model by visualizing the motion of tracer fibers in an index-of-refraction matched suspension. The orientation distribution function is determined experimentally as a function of channel height. The results indicate that at distances less than one half fiber length from the channel walls, the model accurately predicts the available fiber orientation states and the distribution of fibers amongst these states. The model further predicts a sharp concentration gradient in this region.

1 INTRODUCTION

In this work, we implement the wall boundary condition model proposed by Schiek & Shaqfeh [1] to study the behavior of non-Brownian, rigid fiber suspensions flowing through a rectangular channel, see Figure 1. The case considered here is for flow with semi-dilute suspensions consisting of rigid rods suspended in a viscous, Newtonian fluid. The Reynolds number, *Re*, based on the fiber length is asymptotically small, and based on the channel height is order one.

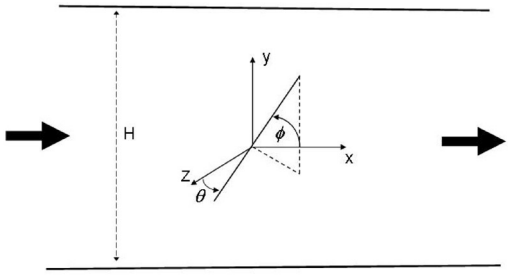

Figure 1. The channel geometry and fiber orientation angles used in this study. The large arrows indicate the direction of flow.

Fiber orientation is key to understanding the strength properties of paper. The desired orientation state is not unique for each product or grade and is set for each particular application. It is widely known that fiber orientation in paper depends largely on the suspension flow through the headbox. Some of the factors which influence flow in the headbox include the local fiber concentration and orientation state as well as the local flow field inside the headbox nozzle [2]. Olson *et al.* [3] showed that fiber alignment can be increased by simply increasing the contraction ratio of the headbox, while Hyensjö *et al.* [4] showed that fiber alignment can be reduced by strategically positioning turbulence generating vanes about the headbox nozzle. The fiber orientation model used in these studies has provided valuable insight into the design of the headbox. However, these works have two major short-comings, namely that they do not account for fiber-wall interactions nor do they capture concentration gradients in the fiber suspension.

Theoretical developments in fiber suspension rheology have shown that the rotary motion of a single, freely suspended fiber in a moving fluid depends largely on local velocity gradients in the flow. Jeffery [5] was the first to formally prove this relationship. By using a no-slip boundary condition along the surface of a fiber and matching the velocity field in the region near the fiber to the bulk flow field of the suspending medium, Jeffery derived an expression for the angular velocity. His derivation showed that a single fiber will rotate continuously in one of an infinite set of closed orbits around the vorticity axis. Bretherton [6] advanced the argument that Jeffery's equations apply to cylindrical particles if the particle aspect ratio, r, is replaced by an effective aspect ratio. This was confirmed experimentally by Goldsmith & Mason [7].

It is well know that as the fiber concentration increases, deviations are observed from Jeffery's predictions. The discrepancy stems from the fact that fibers interact with neighboring fibers hydrodynamically at distances on the order of a fiber length, L. Folgar & Tucker [8] addressed this issue by modeling fiber-fiber interactions as a diffusional process and defined an empirically determined rotary diffusion coefficient, D_r. They proposed, through dimensional analysis, a simple relationship in which D_r is linearly proportional to the magnitude of the rate of strain tensor, $|\mathbf{E}|$. For two dimensional flow in a linear contraction, D_r can be expressed as

$$D_r = C_I \|\mathbf{E}\| \tag{1}$$

where C_I is traditionally called the interaction coefficient and is related to suspension parameters such as concentration, aspect ratio, and fiber length.

Fiber suspension flow is complicated further by the fact that the flow field of the carrier fluid responds to the fiber orientation state. The result is a two way coupling between the fiber orientation state and the flow field. The first to address this issue was Batchelor [9] who developed a general constitutive equation for the bulk stress in a suspension of rigid, inertialess particles of arbitrary shape in a Newtonian fluid. By representing a single particle in suspension as a distribution of Stokeslets[1] over a line enclosed by the particle body, Batchelor determined expressions for the resultant force required to sustain translational motion and the resultant couple required to sustain rotational motion. Dinh & Armstrong [10] extended Batchelor's theory to account for the orientation state of elongated particles and its effect on the bulk stress within the suspension. This was accomplished by assuming that the orientation state of the suspension can be completely described by a known orientation distribution function, ψ, such that the probability of finding fibers oriented between the angles ϕ and $\phi + \partial\phi$ is $\psi(\phi)\partial\phi$. By linearizing the flow field around the particle they were able to equate Batchelor's constitutive equation to a new constitutive equation; one that is proportional to the fourth order moment tensor of ψ. The proportionality constant is referred to as the effective viscosity of the suspension. Bibbo, Dinh & Armstrong [11] validated the work of [10] by experimentally measuring the shear stress within a semi-concentrated suspension undergoing simple shear flow. Their measurements demonstrated a strong coupling between fiber alignment and the resulting shear stress within the suspension and that the Dinh-Armstrong model was suitable for predicting the additional fiber stress. Shaqfeh & Fredrickson [12] derived asymptotic expressions for the effective viscosity of dilute and semi-dilute suspensions of rods in a Newtonian fluid. For semi-dilute fiber suspensions, they express the fiber stress as follows

$$\boldsymbol{\tau}^{fiber} = \frac{\mu c r^2 \mathbf{E} : \langle \mathbf{pppp} \rangle}{ln(1/c) + ln(ln(1/c)) + 1.439} \tag{2}$$

where c is the volume fraction of fibers in the suspension, μ is the viscosity of the suspending fluid and $\mathbf{E}$ is the fluid strain rate tensor, defined as
The remaining term that needs to be defined in Equation 2 is the fourth order

$$\mathbf{E} = (\nabla \mathbf{u} + \nabla \mathbf{u}^{\mathbf{T}}) \tag{3}$$

[1] A Stokeslet is defined as a singularity in a Stokes flow which represents the resultant effect of a force applied to a fluid at that point.

moment of the orientation distribution function Ψ. It is often referred to as the fourth order orientation tensor and is defined as

$$\langle \mathbf{pppp} \rangle = \int p_i p_j p_k p_l \Psi(\phi) d\phi \tag{4}$$

where **p** is a unit vector pointing in the direction parallel to the axis of the fiber, that is

$$\mathbf{p} = \begin{bmatrix} \cos\phi \sin\theta \\ \sin\phi \sin\theta \\ \cos\theta \end{bmatrix} \tag{5}$$

where ϕ is the projected angle of the fiber in the xy-plane and θ is the angle between the fiber and the z-axis, see Figure 1.

The Eulerian description of fiber suspensions is a natural choice for the implementation of Equation 2. With this approach, the suspension is treated as a continuum and the position and orientation of the fibers are described by a probability density function. The main advantage of the Eulerian method is that it is computationally more efficient than particle level simulations, as the latter requires solving for the motion for each particle in the suspension. Further, it has the potential to account for the complex fiber-fiber interactions and the modification of the flow field by the presence of the fibers. However, the Eulerian method does have a number of shortcomings. Specifically, the Eulerian method is unable to model mechanical interactions, either with walls or with other fibers in the suspension. Another issue is that the Eulerian method can not describe the detailed motion of any individual fiber. For example, it is common to find real fibers in a so-called 'flipping' state, i.e. fibers that rotate continuously by 180° about its center. Yet, for many engineering applications, the Eulerian method is able to predict the state of a suspension adequately. With the Eulerian description, the probability of fibers having orientation **p** and position **r** at time t is denoted as $\Psi(\mathbf{r},\mathbf{p},t)$. The convection-diffusion model which governs the evolution of Ψ is given by [3]

$$\frac{\partial \Psi}{\partial t} = D_r \nabla_r^2 \Psi - \nabla_r \cdot (\boldsymbol{\omega} \Psi) + D_t \nabla^2 \Psi - \nabla \cdot (\bar{\boldsymbol{V}} \Psi), \tag{6}$$

where $\overline{\mathbf{V}}$ is the mean translational velocity of the fibers, $\boldsymbol{\omega}$ is the fiber's angular velocity, and ∇_r is the rotational operator expressed as

$$\nabla_r = \boldsymbol{p} \times \frac{\partial}{\partial \boldsymbol{p}} \tag{7}$$

The fiber's angular velocity, $\boldsymbol{\omega}$, is related to the fibers rotational vector by the following expression,

$$\boldsymbol{\omega} = \mathbf{p} \times \dot{\mathbf{p}} \tag{8}$$

D_t and D_r are the translational and rotational diffusion coefficients. In laminar, semi-dilute suspension flows, D_r considers the rotational diffusivity resulting from fiber-fiber interactions (e.g. [8, 13–16]). In turbulent flows, D_r models the rotational diffusivity resulting from turbulent fluctuations in the flow (e.g. [17–19]). D_t plays a similar role to D_r in that it models the spatial diffusion of Ψ; this term may lead to concentration gradients in the suspension. For laminar flows, D_r is typically on the order of $10^{-1} - 10^{-2}$ (e.g. [8, 20, 32]) while $D_t \ll D_r$. Rahnama *et al.* [21] have shown that for the laminar flow of a semi-dilute suspension of rods, D_t is on order $O\left(10^{-3}\frac{\gamma L^2}{ln^2 r}\right)$. For papermaking fibers we see that D_t would be of the order $10^{-5} - 10^{-6}$.

With the assumption, $0 < D_t \ll 1$, many researchers using the Eulerian method, often neglect the spatial diffusivity term and assume that fibers are uniformly distributed throughout the domain (e.g. [8, 14, 15, 18, 22, 23]). This simplification is well justified for unbounded flows, or when computing Ψ far enough away from channel walls. However, by assuming $D_t \to 0$ over the entire domain, the problem formulation is altered considerably. For example, when the spatial diffusivity is neglected, Equation 6 is reduced from second order in space to first order and requires one fewer set of boundary conditions in the spatial domain. Further, since $D_t \ll 1$, there is a possibility for boundary layers to exist near the channel walls. Since one set of the boundary conditions are eliminated, it may not be possible to obtain an accurate solution to Equation 6 over the entire spatial domain.

Experimental evidence has demonstrated that fibers behave quite differently near solid boundaries compared to their behavior in central parts of a channel. Stover, & Cohen [25] appear to be the first to rigorously address this issue experimentally. In their studies, the motion of rodlike particles in a low Reynolds number plane Poiseuille flow were observed experimentally and the effect of the wall on the period of fiber rotation was determined. They found that when particles with a high Jeffery orbit constant, that is particles with a large period of rotation about the vorticity axis, came within a distance less than half a fiber length from the wall, an irreversible interaction between the fiber and wall occurred where the fiber was said to "pole-vault" away from the wall to a distance of approximately half a fiber length. This interaction was named accordingly as it seemingly mimicked the flipping motion of pole-vaulter. Yet the fiber was said to never actually touch the wall but rather that

the fiber tip would come within approximately one fiber diameter from the wall. They suggested the existence of some nonhydrodynamic force between the fiber and wall but could not determine the exact nature of this interaction. They observed quite a different behavior for fibers with a low Jeffery orbit constant that came within a half fiber length from the wall. In this case, the fiber remained close to the wall indefinitely. If the fiber had a period of rotation somewhere between these extremes it shifted its orientation away from the wall. In studies by Moses *et al.* [26], the rotational and translational motion of a single fiber near a solid boundary was measured experimentally in a planar shear flow apparatus. These studies showed that for locations less than a fiber length from the wall, fibers rotate to position themselves parallel to the wall and remain in this orientation indefinitely. They concluded that for these fibers, the wall has a stabilizing effect on the fiber.

Capturing the unique, near wall behavior of fiber suspensions using an Eulerian description is not a trivial matter. The simplest, and most easily satisfied wall boundary condition for Ψ is a simple no-flux condition, i.e., fibers, and hence Ψ, cannot be transported through solid walls. This condition is naturally satisfied by the no-slip and no-penetration conditions for the fluid along a wall. Further, it is both sensible and straightforward to apply this to spherical particles. However, for elongated, orientable particles, the no-flux condition is not so simple. For example, if the center of a fiber is positioned at a distance less than half its length away from a wall, the fiber is not free to assume all possible orientations. This suggests the existence of a set of forbidden orientation states, i.e. those orientations which are unrealistic.

This problem was formally addressed by Schiek & Shaqfeh [1], who used geometric arguments to derive a set of necessary boundary conditions for Ψ near rigid channel walls. They went on to apply these boundary conditions to the flow of non-dilute, Brownian suspensions and showed that the surface over which the zero flux boundary condition must be satisfied is not simply that of the wall, but rather a complex hyper-surface that forbids any part of the fiber from penetrating the wall. Explicitly, this can be expressed as follows

$$\boldsymbol{n} \cdot (\boldsymbol{j}_r + \boldsymbol{j}_t) = 0 \tag{9}$$

where **n** is the local, unit normal to the hyper-surface separating the allowed and forbidden fiber orientation states. $\boldsymbol{j}_r$ and $\boldsymbol{j}_t$ are respectively the rotational and translational flux of the probability density function, Ψ, i.e.

$$\boldsymbol{j}_t = D_t \nabla \Psi - (\bar{\boldsymbol{V}} \Psi) \tag{10}$$

$$\boldsymbol{j}_r = D_r \nabla_r \Psi - (\boldsymbol{\omega} \Psi) \tag{11}$$

In words, Equation 9 states that any rotational flux that places one end of the fiber into the wall must be balanced by a translation flux which moves the center of the fiber away from the wall. This argument might also be one underlying mechanism which leads to non-uniform concentrations in this near wall region, a phenomenon previously reported by other researchers (e.g. [27, 28]). The rigorous formulation of the no-flux boundary conditions for Ψ presented here has been used by other researchers (e.g. [29, 30]), however these studies were numerical in nature and investigate the flow of Brownian suspensions. Further, experimental validation of these boundary conditions do not appear in the literature, nor do they appear to have been applied to the flow of non-Brownian suspensions.

In this work, we investigate the rigorous formulation of the no-flux boundary conditions described by Schiek & Shaqfeh [1] with application to non-Brownian, rigid fiber suspension flow through a rectangular channel. We do so by comparing numerical calculations of the probability density function used to describe the local orientation and concentration state of the suspension to experimental measurements at two different concentrations. In §2, we formulate the numerical model along with a derivation of the boundary conditions as they apply to this particular flow. In §3, we measure the orientation distribution of tracer fibers in an index-of-refraction matched solution of rigid glass rods suspended in a viscous Newtonian fluid as a function of distance across the channel. Discussion of the results of this study are given in §4.

2 PROBLEM FORMULATION

The flow is described in the channel using Cauchy's momentum equations for a steady, quasi-1D, incompressible, Newtonian fluid, that is

$$\nabla \cdot \mathbf{u} = 0 \tag{12}$$

$$\nabla P = \nabla \cdot \boldsymbol{\tau} \tag{13}$$

where P is the pressure and τ is the stress tensor, that is the sum of both the Newtonian fluid and fiber contributions

$$\boldsymbol{\tau} = \mu(\nabla \mathbf{u} + \nabla \mathbf{u}^T) + \boldsymbol{\tau}^{fiber} \tag{14}$$

The contribution from the fiber phase to the total stress in the suspension

flow is given by Equation 2. It depends on the local orientation state of the suspension which is described by the probability density function, Ψ. The model for fiber orientation is described in the following section.

2.1 Fiber orientation model

We consider suspensions consisting of rigid rods with length, L, and diameter, d, suspended in a Newtonian fluid. The fibers are assumed to be neutrally buoyant and interact hydrodynamically with each other and with the fluid. It is further assumed that the length scale of the fibers is small enough that the velocity field varies linearly across the length of the fiber. The concentration of the suspension is semi-dilute which is defined through the following relationship (e.g. [31]):

$$1 \leq nL^3 \leq \frac{L}{d} \tag{15}$$

where n is the number density of fibers in the suspension, that is, the number of fibers per unit volume. At distances greater than $\frac{L}{2}$ from the wall, fibers are assumed to be uniformly distributed throughout the suspension. However, we do not make this assumption for distances less than $\frac{L}{2}$ from the walls. The Reynolds number, based on the fiber length is asymptotically small which implies that inertial effects on the scale of the fiber length are negligible. It is further assumed that the center of a fiber translates with the local fluid velocity. To further simplify the problem, we consider a 2D flow and a 2D planar model of fiber orientation where each fiber is assumed to be oriented in the xy-plane with an orientation described by the single angle ϕ. While this is not actually true in theory, where the rotary diffusion term creates out-of-plane orientation in planar flows, the flow field is idealized as planar which implies the fiber orientation in the θ direction will be symmetric about $\theta = \frac{\pi}{2}$ (e.g. [19]). With this, the fiber orientation vector in the xy-plane is defined as follows

$$\mathbf{p} = \begin{bmatrix} \cos\phi \\ \sin\phi \end{bmatrix} \tag{16}$$

For a steady, fully developed flow in the x-direction, Equation 6 can now be

expressed in terms of the orientation angles, ϕ and the x-velocity component, u, i.e.

$$D_t \frac{\partial^2 \Psi}{\partial y^2} = \frac{\partial(\dot{\phi}\Psi)}{\partial \phi} - D_r \frac{\partial^2 \Psi}{\partial \phi^2} \tag{17}$$

Olson *et al.* [3] derived the following relationship for the angular velocity of the fiber in the xy-plane

$$\dot{\phi} = -\frac{\partial u}{\partial y} \sin^2(\phi) \tag{18}$$

Equation 18 is general for a fiber rotating in a linear field and is identical to that derived by jeffery [5] for fibers of large aspect ratio. Six boundary conditions are required in order to obtain an exact solution to Equation 17. Since the ends of a fiber are indistinguishable, periodic boundary conditions are enforced with respect to the orientation angle, ϕ, i.e.

$$\Psi(y, \phi) = \Psi(y, \phi + \pi) \tag{19}$$

Since Ψ is a distribution function, a third boundary condition stems from a normalization constraint. In general, this constraint requires that, when integrated over all the allowable orientations within a volume, V, of the suspension, the probability density should equal the total number of fibers within that volume, N, i.e.

$$\int_V \int_{\phi_1(y)}^{\phi_2(y)} \Psi d\phi dV = N \tag{20}$$

where ϕ_1 and ϕ_2 refer to the minimum and maximum allowable values in ϕ that a fiber may have with its center at a distance y_c from the wall. These values vary with distance from the wall as follows

$$\phi_1(y) = \begin{cases} -\pi/2, & y \geq 1, \text{ and } y \leq H \\ arcsin(y), & y \leq 1 \\ arcsin(H - y), & y \geq (H - 1) \end{cases} \tag{21}$$

$$\phi_2(y) = \begin{cases} \pi/2, & y \geq 1, \text{ and } y \leq H \\ arcsin(-y), & y \leq 1 \\ arcsin(y - H), & y \geq (H - 1) \end{cases} \tag{22}$$

For the system considered here, there is no variation in the x or z-directions, therefore Equation 20 can be simplified by performing the integration over an arbitrary slice in the xz-plane of area, A_{xz} and integrating from the lower channel wall, $y = 0$ to the upper channel wall, $y = H$. With this assumption, the normalization constraint can be expressed as follows

$$\int_0^H \int_{\phi_1(y)}^{\phi_2(y)} \Psi d\phi dy = \frac{N}{A_{xz}} = nH \tag{23}$$

The remaining four boundary conditions result from the no-flux condition on Ψ near the channel walls. For the geometry and assumptions considered here, the no-flux condition at the channel walls is expressed as follows

$$D_t \frac{\partial \Psi}{\partial y} \pm \left(\dot{\phi}\Psi - D_r \frac{\partial \Psi}{\partial \phi} \right) = 0 \tag{24}$$

on $y = \pm \frac{L}{2} \sin\phi$, and

$$D_t \frac{\partial \Psi}{\partial y} \mp \left(\dot{\phi}\Psi - D_r \frac{\partial \Psi}{\partial \phi} \right) = 0 \tag{25}$$

on $y = H \pm \frac{L}{2} \sin\phi$

To re-iterate, the conditions defined by Equations 24 and 25 state that for a fiber in contact with a wall, translational and rotational motions must be coupled in order to prevent a fiber from rotating or translating through the wall, see Figure 2.1.

2.2 Numerical implementation

Numerical computations are carried out for the flow of semi-dilute fiber suspensions of concentration $nL^3 = 3.6$ and $nL^3 = 10.8$, or equivalent volume fraction $c = 1.1 \times 10^{-3}$ and $c = 3.3 \times 10^{-3}$. The channel geometry is shown in Figure 1 where we use a channel height, $H = 50$ *mm*. Based on the measurements of krochak *et al.* [32], we set $C_I = 0.003$ and $C_I = 0.004$. These values correspond to concentrations $nL^3 = 3.6$ and $nL^3 = 10.8$ respectively. D_t is held constant at $D_t = 0.0001$ [21].

The computational domain consists of a 2D rectangular channel, 2000 *mm*

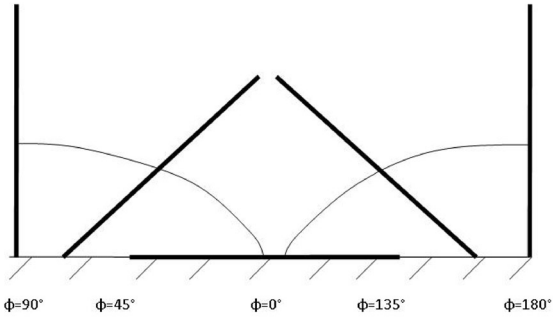

Figure 2. Coupling between translational and rotational motion at a solid boundary.

in length and 50 *mm* in height. In the y-direction, we use a 100-point, uniform mesh of size $\Delta y = 0.0005$, while in the x-direction, a uniform mesh of size $\Delta x = 0.02$, resulting in a 100×100 mesh. The flow field in the channel is computed using a commercial CFD software package, FLUENT (www.fluent.com). The solution to the flow field is obtained using a 2D, segregated, implicit solver, with water at $20°C$ as the fluid phase. A no-slip condition is enforced along the channel walls. At the channel inlet, a parabolic profile is enforced with a peak inlet velocity of 0.01 *m/s* in the x-direction, similar to the centerline velocity used in the experiments. Velocity field data used in solving Equation 17 is extracted along a single, vertical slice far enough downstream of the inlet so that the flow no longer varies in the x-direction.

At distances greater than $\frac{L}{2}$ from the channel walls, Equation 17 is discretized using a second order accurate, centered differences in both the physical and orientation spaces. At the boundaries, specifically along the hypersurface separating the allowable from the forbidden orientation states, Equations 24 and 25 are discretized using forward differences such that the solution marches away from the wall, both in position and in orientation. This results in 4 regions which must be handled separately, each corresponding to one of the two ends of a fiber touching either the top or bottom wall in the channel. Ψ is initialized with a uniform distribution, $\Psi = \frac{1}{\pi}$ after which Equations 17–25 are solved iteratively with a Gauss-Seidel method until the solution residual is less than 10^{-6}.

In order to couple the momentum equations to the fiber orientation

equations, an iterative procedure is used whereby the flow field is initially determined for the pure fluid, that is water with no fibers, after which Equations 17 and 18 are solved using the initial flow field data. The contribution of the fiber phase to the total stress on the fluid is defined by Equation 2 and is computed upon solving the orientation equations for Ψ. Once computed, the gradient of the fiber stress is determined and then treated as a momentum source term in the fluid momentum equations. This source term is implemented in Fluent by means of a so-called User Defined Function written in C. The fluid flow equations are then solved again to produce a new flow field. On each iteration, the flow field is deemed to be converged when the L_2 norm of the solution residual is less than 10^{-6}. The process is repeated until the change in the L_2 norm of the velocity vector between successive iterations is less than 10^{-6}. In general, a total of four iterations of each of the flow field equations, and of the orientation equations were required to obtain a fully converged solution.

3 EXPERIMENTAL PROCEDURES

An index-of-refraction matched suspension, that is, a suspension consisting of fluid and fiber phases with identical indexes of refraction, is used to measure the orientation distribution function in an experimental channel. With this type of system, the fiber phase becomes indistinguishable from the fluid phase when observed under white light. A small number of fibers (less than 1% of the total number of fibers) are then silvered and their motion is visualized in the flow using a digital camera in conjunction with an automated fiber tracking program. The motion and orientation of the observed fibers are assumed to represent the behaviour of all fibers within the suspension.

The experiments were performed in a rectangular cross-sectional Plexiglas cell of size 50 $mm \times 255$ $mm \times 75$ mm (inlet height × length × width) proceeded by a hyperbolic contracting section used to stabilize the flow and remove any cross-flow, see Figure 3. Approximately 2.0 l of suspension was required to fill the channel. Up- and downstream of the channel are reservoirs set at different heights to control the pressure drop over the cell. The flow rate was set at $4.25 \times 10^{-5} m^3/sec$ using a gravity feed on the inlet side.

Borosilicate glass rods (www.mosci.com) of dimensions 5 $mm \times 0.1$ mm (length × diameter) were employed as the fiber phase. The glass fibers had a density of approximately 2250 kg/m^3. The index of refraction of these fibers was measured commercially and found to be 1.4719(±0.0005). Approximately 0.01% of the fibers in each suspension were silvered using Tollen's solution, a mixture of 5 ml of 0.1 M $AgNO_3$ with ~ 10 μL (5 drops) of 0.4 M

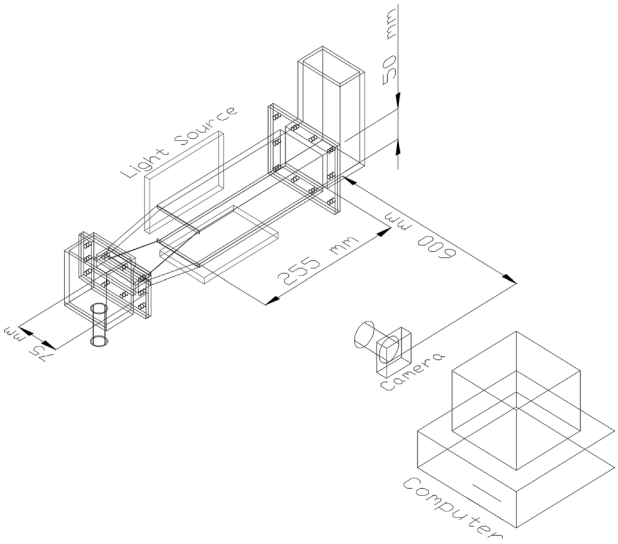

Figure 3. A schematic diagram of the experimental test section. Fiber orientation is observed immediately prior to the contracting section.

NaOH. Before silvering, the fibers were washed in detergent, rinsed in alcohol and then in distilled water. After silvering the fibers were washed to remove any loosely adsorbed $AgNO_3$. We measured the motion and orientation of 2 different monodispersed suspensions of concentration, $nL^3 = 3.6$ and $nL^3 = 10.8$. The Newtonian fluid used in this system was glycerin with a density of 1260 kg/m^3, a viscosity of 1.49 *Pa s* and an index of refraction of 1.470. Fiber settling was not observed over the time-scale of the experiment. The suspension was stirred for several minutes using variable frequency drive mixer (Midwest Mixing Corp.) until the fibers were uniformly distributed throughout the suspension.

Our visualization system consisted of a progressive scan Basler A201b monochrome CCD camera (10 bit grey scale and 1008 × 1016 pixel spatial resolution with a maximum framing rate of 30 frames per second), mounted with an F-mount Micro-NIKKOR 105 *mm* lens, positioned 60 *cm* in front of the observation section. The imaged area was 50 *mm* × 50 *mm* with a resolution of approximately 50 *μm/pixel*. All images were captured immediately prior to the contracting section of the experimental channel.

For particle tracking, the lens aperture and focus, backlight intensity and camera exposure time were chosen so that the whole imaged volume was within the depth of field of the lens. The camera was focused in the middle of

the xz-plane in an attempt to avoid measuring the orientation of fibers near the side walls. The plexiglass cell was transilluminated using Schott-Fostec fiber optic dual backlight. One backlight was positioned behind the observation section and one was placed below the observation section. The orientation of each particle was calculated using an in-house fiber tracking algorithm and consists of the following subroutines:

1. *Particle identification* – Particle edges are detected using a Prewitt edge detection scheme with the original greyscale image converted to a binary image. Particle edge pixels are set to white (pixel value of 1) on a black background (pixel value 0). Particles are then dilated, the interior regions filled with white pixels, and then eroded back to their original size. The image now contains filled white particles on a black background. Any object whose length and width are less than 10 pixels in size, or whose length and width are approximately equal are assumed to be artifacts in the image (e.g. air bubbles or non-fibrous debris) and are removed from the image. In addition, stationary objects were removed from the images.
2. *Orientation Distribution* – The orientation angle of each fiber is measured relative to the horizontal by computing the arctangent of the ratio $\frac{\Delta y}{\Delta x}$ between the end points of a fiber. The associated fiber length and center of area is also recorded. The flow region is then partitioned into $5mm \times 5mm$ cells and the orientation angle of each fiber whose center of area lies within a particular cell is computed. There were on average approximately 5000 tracer fiber observations at each location for each experiment.

Figure 4 shows an example of an original image and the same identical after processing.

4 RESULTS AND DISCUSSION

In this section, numerical predictions of the orientation distribution function are compared with experimental observations across the channel gap. We present first our results on the orientation state of the suspension in the near wall region, i.e. the region within $\frac{L}{2}$ from the channel walls. To re-iterate, we argue that a rigorous formulation of the boundary conditions on Ψ must be enforced in this region and it will be shown that the no-flux boundary conditions described by Equations 24 and 25 describe accurately the fiber

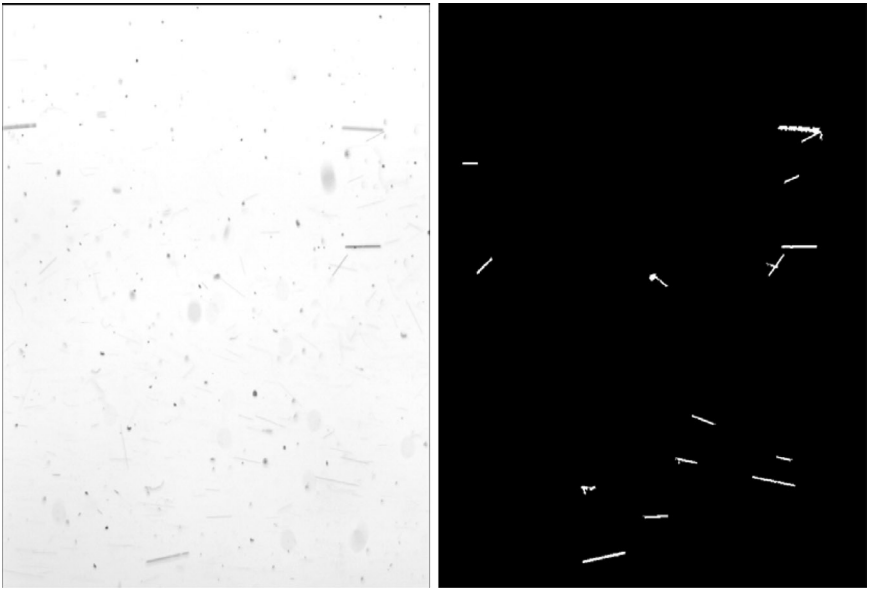

Figure 4. An example of an original image (left) and a post-processed image with white fibers on a black background (right).

orientation state in this region. A general orientation analysis will also be performed for distances greater than $\frac{L}{2}$ from the walls where all orientation states are physically possible and the system is well described by Equation 17. We follow this with a comparison of concentration profiles across the channel.

Before proceeding to the main findings of this section, it is instructive to first characterize Ψ for the experimental conditions tested. An example of the orientation distribution at the channel centerline is shown in Figure 5. Included in this figure is a comparison of the experimental data. The histogram of the orientation distribution function in this part of the channel was found to be smooth and clustered around a definite value, $\phi = 0$. However in the experiments, many fibers were observed to be oriented at angles well away from $\phi = 0$, specifically near $\phi = 1$ *rad*. These observations correspond to 'flipping' fibers, one particular phenomenon that the Eulerian model is unable to capture.

We now turn to the main findings of this work, namely an evaluation of the

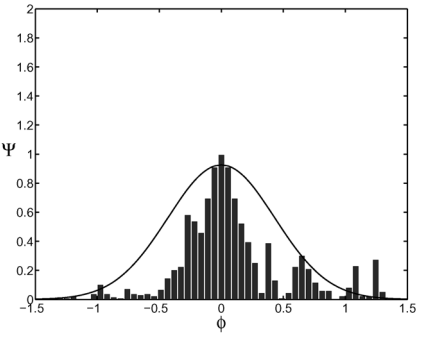

Figure 5. The orientation distribution at the channel centerline, $y/H = 0.5$. The concentration shown here is $nL^3 = 3.6$, the fiber length is 5 *mm*, and aspect ratio is 50.

orientation distribution function at distances less than $\frac{L}{2}$ from the channel walls. Shown in Figure 6 is a comparison of the numerical predictions with the experimental measurements. Here we compare results for $nL^3 = 3.6$, however similar results were found for $nL^3 = 10.8$. The model agrees well with the experiments in this region, although it does over predict fiber orientation closest to the wall. The most notable observation is that the model is able to capture the range of allowed orientation states in this region. Very close to the wall, specifically at distances within approximately 1 *mm* of the wall, Figures 6 (a) and (b) show that nearly all fibers are aligned parallel to the wall, i.e. Ψ is highly clustered about $\phi = 0$, a result which stems from the tight geometric constraint on fiber orientation in this region. Moving slightly farther away from the wall, but still in the region $y < \frac{L}{2}$, Figures 6 (c), (d) and (e) show that the peak in Ψ begins to shift toward positive values in ϕ, while the spread in Ψ begins to increase significantly. The increased spread in Ψ indicates that fibers have more freedom to rotate in this region and therefore assume a greater range of orientations. However, the preferred direction of fiber orientation points away from the wall. The model agrees very well with the experiments in this region, both qualitatively and quantitatively and does an excellent job at separating the allowed from the forbidden orientation states. Moving further from the wall still, Figure 6 (f) shows the the point at which all orientation states are theoretically allowable, i.e. at the point $y = \frac{L}{2}$. Here, the peak of Ψ corresponds to a positive value in ϕ, which again

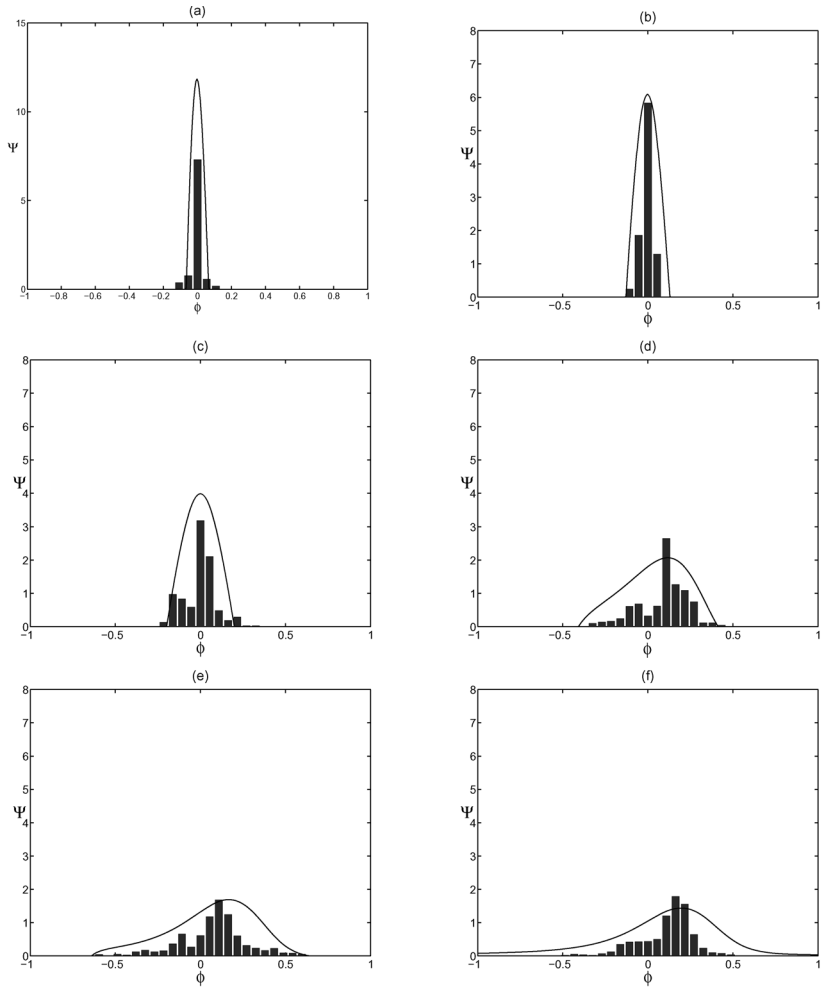

Figure 6. The orientation distribution at various distances in the near wall region. (a) $y/L \to 0$, (b) $y/L = 0.1$ ($y/H = 0.01$), (c) $y/L = 0.2$ ($y/H = 0.02$), (d) $y/L = 0.3$ ($y/H = 0.03$), (e) $y/L = 0.4$ ($y/H = 0.04$), (f) $y/L = 0.5$ ($y/H = 0.05$). The concentration shown here is $nL^3 = 3.6$, the fiber length is 5 *mm*, and aspect ratio is 50.

indicates a tendency for fibers to point away from the wall. Furthermore, since fiber orientation is no longer restricted geometrically by the wall, the spread in Ψ encompasses all orientation states.

To fully characterize the fiber orientation distribution across the channel,

we consider two measures of the orientation distribution function, namely the mean orientation angle, $\overline{\phi}$, and the orientation anisotropy, A_ϕ. The mean orientation angle corresponds to the principal direction of fiber alignment, i.e. the angle at which the majority of fibers are oriented. The orientation anisotropy corresponds to the degree of fiber alignment about the principal direction of orientation. As a reference, a value of A_ϕ equal to unity corresponds to a perfectly aligned suspension, where as a value of $A_\phi = 0.5$ corresponds to a suspension that is in a fully random, or uniform orientation state. $\overline{\phi}$ and A_ϕ are defined respectively as follows

$$\bar{\phi} = \int_{-\frac{\pi}{2}}^{\frac{\pi}{2}} \phi \Psi(y, \phi) d\phi \tag{26}$$

and

$$A_\phi = \int_{-\frac{\pi}{2}}^{\frac{\pi}{2}} \Psi cos^2 \phi d\phi \tag{27}$$

Figure 7 compares predicted profiles of $\overline{\phi}$ with experimental measurements, where the error bars indicate the 95% confidence interval. Here we see that in the lower half of the channel and at distances greater than $\frac{L}{2}$, the mean

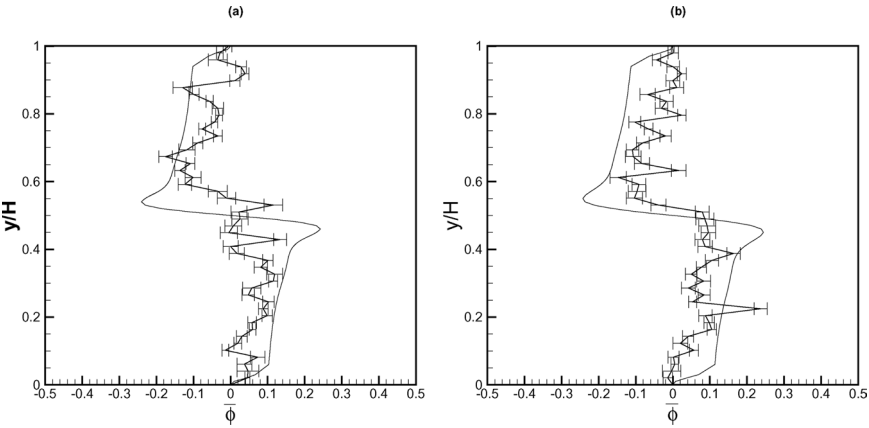

Figure 7. Comparison of the mean orientation angle across the channel. Shown here are the model predictions along with the experimental observations for $nL^3 = 3.6$ (a) and for $nL^3 = 10.8$ (b). The error bars indicate the 95% confidence interval.

direction of fiber alignment is positive, i.e. fibers in the lower half channel tend to point away from the lower wall toward the upper wall. Similarly in the upper half channel and at distances greater than $\frac{L}{2}$, the mean direction of fiber alignment is negative, i.e. fibers in this region point away from the upper wall and toward the lower wall. These findings are due to the fact that fiber alignment is predominantly driven by local velocity gradients. In the lower half channel, the velocity gradient, $\frac{\partial u}{\partial y}$, is positive and fibers tend to align in the positive direction. Similarly, in the upper half channel, the velocity gradient is negative and fibers are aligned in the negative direction. Along the centerline, the mean fiber orientation is at $\phi = 0$, or parallel to the x-axis. At distances less than $\frac{L}{2}$, the mean fiber orientation angle increases from $\overline{\phi} = 0$ closest to the wall, to $\overline{\phi} \approx 0.1$ *rad* at $y = \frac{L}{2}$.

Profiles of are compared in Figure 8, where the error bars indicate the 95% confidence interval. The model is able to give a good qualitative prediction of the character of A_ϕ across the channel. Specifically, A_ϕ is at a maximum closest to the channel walls where it tends toward a value of 1, indicating that all fibers in this region are aligned parallel to the walls. A_ϕ then decreases

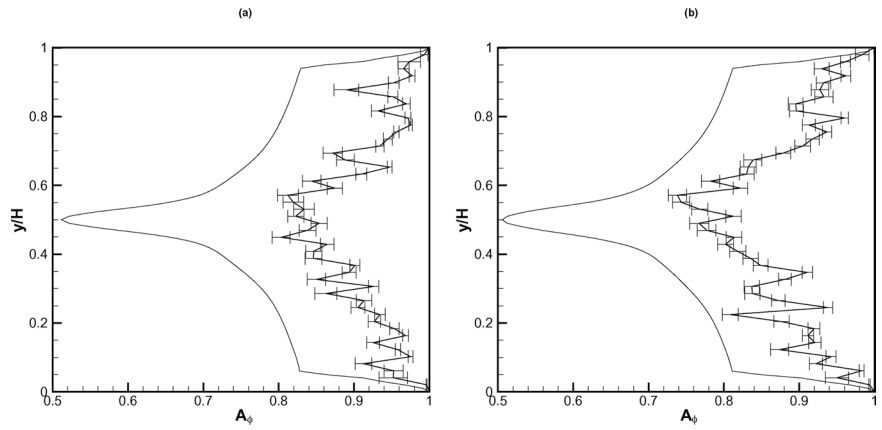

Figure 8. Comparison of the orientation anisotropy across the channel. Shown here are the model predictions along with the experimental observations for $nL^3 = 3.6$ (a) and for $nL^3 = 10.8$ (b). The error bars indicate the 95% confidence interval.

non-linearly to a minimum value at the center of the channel where the suspension is at its most random in orientation. This finding re-enforces the notion that the wall increases fiber alignment in the near wall region. This result agrees well with the experimental findings of [26] and [25], where the wall was said to have a stabilizing effect of fiber orientation at distances less than $\frac{L}{2}$. Close to the walls, the model agrees quantitatively and qualitatively with the experimental observations. However, away from the walls, the model only agrees in character and quantitative agreement is not as strong. The quantitative ambiguities can most likely be accounted for by the fact that here we have assumed a planar orientation of fibers in the numerical model, i.e., fiber alignment is assumed to be entirely in the *xy*-plane. However, in the experiments, fiber alignment is not limited to the *xy*-plane and fibers are free to rotate in the out-of-plane direction. This is most certainly one major source of error here. In all cases, the numerical model is able to capture the character of A_ϕ across the channel, particularly closest to the walls, something which would not otherwise be possible without implementing the rigorous no-flux boundary conditions on Ψ.

The effect of increasing the fiber concentration appears as a reduction in A_ϕ across the channel, particularly along the channel centerline. This result is due to the fact that increasing the fiber concentration effectively increases the rotary diffusivity caused by the fiber-fiber interactions. More specifically, with a greater number of fibers confined to the same domain, the frequency of fiber-fiber interactions is increased and the suspension tends to be less aligned. This observation has been previously reported by a number of different researchers (e.g. [16, 32–34]). The model also predicts an increase in A_ϕ for the $nL^3 = 10.8$ suspension, however this is expected since we have assigned a larger value of C_I to this case.

At this point, it is worth commenting on the oscillations which appear in the measurements of both $\overline{\phi}$ and A_ϕ across the channel. This is believed to be a result of hydrodynamic fiber-fiber interactions and an indication that fibers are beginning to flocculate. We put fourth the argument that fibers are segregating into small flocs, where the orientation state of each floc may differ slightly from that of neighboring flocs. Further, it has previously been shown that fiber suspension flow at low Reynold's number can be characterized as having a plug-like velocity distribution with minimal velocity gradients in the plug region (e.g. [36]). Since velocity gradients are low in the plug region, so too is the aligning force in this region and the orientation state of the suspension is largely determined by the orientation state at the channel inlet and by the fiber-fiber interactions.

Now we compare concentration profiles in the suspension flow across the

channel gap. In the experiments, we assume the number of observed tracer fibers at an observation point is indicative of the fiber concentration at that point. It should be pointed out that our fiber visualization system does not consider fibers that are oriented, almost entirely, in the *xz*-plane. However, the number of fibers which are completely oriented in the *xz*-plane is small and should not have a significant impact of the measured concentration distribution. In the theory, the probability, P_{cm}, of finding a fiber with its center at any point, y, is defined as

$$P_{cm}(y) = \int_{\phi_1(y)}^{\phi_2(y)} \Psi(y, \phi) d\phi \tag{28}$$

where $\phi_1(y)$ and $\phi_2(y)$ are defined in Equations 21 and 22 respectively. A comparison of the predicted P_{cm} with the experimentally observed concentration profile is shown in Figure 9, where P_{cm} has been scaled by the fiber concentration, nL^3, and the experimentally observed concentration profile has been scaled by the mean profile at distances greater than $\frac{L}{2}$ from the wall.

Figure 9 shows several interesting findings. First, there is a significant difference in the character in the measured profiles for the two different concentrations. For the case $nL^3 = 3.6$, the profile increases linearly from the wall to a distance of approximately L, after which it appears to increase non-linearly

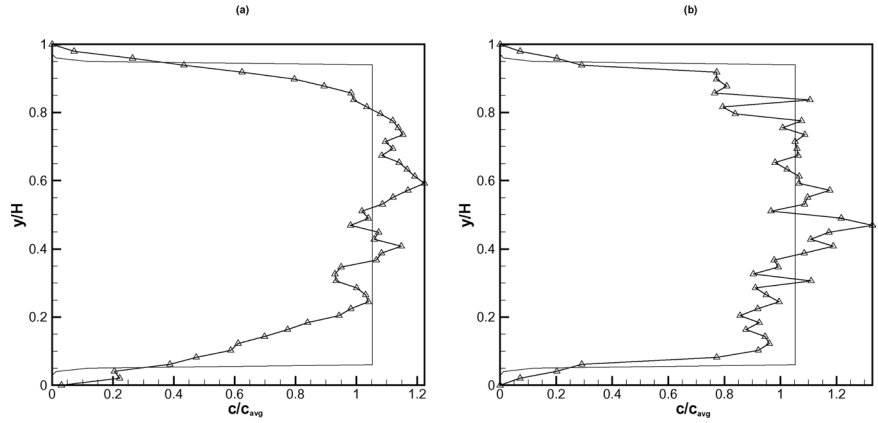

Figure 9. Concentration profiles across the channel. Shown here are the model predictions (–) along with the experimental observations (Δ) for $nL^3 = 3.6$, (a), and for $nL^3 = 10.8$, (b).

with a maximum near the center of the channel. For the case $nL^3 = 10.8$, there is a very small region very near to the channel wall where fiber concentration increases rapidly and non-linearly. Sightly further from the wall, the concentration increases linearly to a distance of approximately $\frac{L}{2}$ from the wall, after which it is essentially constant across the channel. This later behavior is also predicted by the model calculations. However with the model, there is no change to the character of the profile when the concentration is changed. Comparing the model predictions at $nL^3 = 3.6$, this low concentration near the channel walls is predicted to be exactly $\frac{L}{2}$ in size, where as the experiments shows this region to be considerably larger, i.e. on the order of the fiber length, L. Another observation in Figure 9 is that the model predictions of fiber concentration in the central part of the channel is seen to be slightly greater than unity, despite being normalized by the mean concentration. This result is due to the fact that fibers from the depleted, near wall region must accounted for elsewhere in the channel so that the normalization condition, i.e. Equation 23, is satisfied. The oscillations we observe in the experimental measurement are believed to be the result of small scale fiber flocculation. Further, we feel that the oscillations observed in the fiber concentration measurements supports the explanation on the oscillations that were observed in the orientation measurements.

There are still a number of discrepancies between the model predictions and the experimental measurements, most notably, the model over-predicts $\overline{\phi}$ and A_ϕ away from the channel walls. This is likely due to the fact that, in this work, we have considered a 2D model of fiber orientation. However, in the experiments, the fibers have three dimensional orientation and are not limited to rotate solely in the xy-plane. While three dimensional fiber orientation should not change the character of the fiber behavior, it will certainly affect quantitative values of both $\overline{\phi}$ and A_ϕ. One possible cause for discrepancies in the near-wall region may be explained by the flipping fiber phenomenon, and the frequency of fiber flipping in relation to the suspension concentration. More specifically, for the lower concentration suspension, fibers entering the near wall region were observed to flip by 180° (or several multiples thereof) more often compared to the higher concentration suspension. At the low concentration, these flipping fibers were observed to eventually drift to a distance well in excess of $\frac{L}{2}$ from the wall, after which they assumed a stable fiber orientation. At the higher concentration, not only were there far fewer occurrences of flipping fibers, but those which did flip, often remained much

closer to the wall upon stabilizing, i.e. approximately $\frac{L}{2}$ from the wall. Similar observations have also made by [25] and [26], however here we find that at a low concentrations, fibers drift out to distances on the order L after undergoing this pole-vaulting action, where as [25] and [26] found that fibers drifted to a distance of approximately $\frac{L}{2}$ from the wall, even in the dilute limit. Another possible explanation for this observation is that, at low concentrations, fibers have fewer neighbors so that flipping fibers are less likely to mechanically interact with other fibers, allowing them the freedom to drift farther away from the walls. Capturing such detailed fiber behavior is one inherent deficiency with the Eulerian modeling approach. Nonetheless, the Eulerian model used here is able to predict these linear concentration profiles which could arguably result from the flipping fiber phenomenon.

5 CONCLUSION

A numerical model has been presented to predict the orientation and concentration state of rigid fiber suspensions in a bounded channel flow. A rigorous formulation of the wall boundary conditions has been implemented in the model, allowing accurate predictions of fiber orientation across the entire channel and up the channel walls. Measurements of fiber orientation were carried out in an experimental device in order to validate the model. Good qualitative agreement in fiber orientation was found between the model predictions and the experimental measurements across the entire channel. The model agreed particularly well in the near wall region, both qualitatively and quantitatively. Away from the channel walls, good qualitative agreement was shown with the quantitative discrepancies being attributed to our neglecting the out-of-plane fiber orientation in the numerical model. Comparison was also made between the predicted and measured concentration profiles. Both the predicted and measured concentration profiles clearly showed a linear increase in fiber concentration from the channel wall. However, beyond the linear region, the measurements showed different behaviors for the different concentrations. At low concentration, the concentration profile reached a maximum near the center of the channel, where as at high concentration, the concentration profile was approximately constant across the channel. Furthermore, the size of the linear concentration region was shown experimentally to be on the order L at low concentration, and on the order $\frac{L}{2}$ at high

concentration. The model predicted the linear region to be one half fiber length in size, and independent of concentration.

REFERENCES

1. Schiek R.L., & Shaqfeh E.S.G. A Non-Local Theory for Stress in Bound, Brownian Suspensions of Slender, Rigid Fibers *J. Fluid Mech.* **296**:271–324, 1995.
2. Ullmar, M. & Norman, B. Observation of Fiber Orientation in a Headbox Nozzle at Low Consistency *TAPPI Proceedings, Engineering and Papermaking conference*, pp 865–873, Nashville, TN. Tappi Press, Atlanta, 1997.
3. Olson, J.A., Frigaard, I., Chan, C., & Hämäläinen, J. P. Modeling a Turbulent Fiber Suspension Flowing in a Planar Contraction: The One Dimensional Headbox *Int. J. Multiphase Flow* **30**:51–66, 2004.
4. Hyensjö, M., Dahlkild, A., Krochak, P., Olson, J. 2007 Modeling the Effect of Shear Flow on Fiber Orientation Anisotropy in a Planar Contraction *Nordic Pulp Paper Res. J.* **22**, 376–382.
5. Jeffery, G.B. The Motion of Ellipsoidal Particles Immersed in a Viscous Fluid *Proc. Royal Soc. London Series A* **102**:161–179, 1922.
6. Bretherton, F.P. The Motion of Rigid Particles in a Shear Flow at Low Reynolds Number *J. Fluid Mech.* **14**:284, 1922.
7. Goldsmith, H. L. & Mason, S. G. The flow of suspension through tubes I. Single spheres *J. Colloid. Sci.* **17**:448–476, 1962.
8. Folgar, F. & Tucker, C.L. Orientation Behavior of Fibers in Concentrated Suspensions *J. Reinf. Plastics and Comp.* **3**:98–119, 1984.
9. Batchelor, G.K. Slender-body Theory for Particles of Arbitrary Cross-Section in Stokes Flow *J. Fluid Mech.* **44**:419–440, 1970.
10. Dinh, S.M. & Armstrong, R.C. A Rheological Equation of State for Semi-Concentrated Fiber Suspensions *J. Rheol.* **28(3)**:207–227, 1984.
11. Bibbo, M.A., Dinh, S.M. & Armstrong, R.C. Shear Flow Properties of Semi-Concentrated Fiber Suspension *J. Rheol.* **29(6)**:905–929, 1985.
12. Shaqfeh, E.S.G. & Fredrickson, G.H. The Hydrodynamic Stress in a Suspension of Rods *Phys Fluids A* **2**:7–24, 1990.
13. Jackson, W.C., Advani, S.G. & Tucker, C.L. Predicting the Orientation of Short Fibers in Thin Compression Moldings *J. Comp. Mater.* **20**:539–557, 1985.
14. Altan, M.C., Advani, S.G., Güceri, S.I. & Pipes, R.B. On the Description of the Orientation State for Fiber Suspensions in Homogeneous Flows *J. Rheol.* **33**:1129–1155, 1989.
15. Koch, D.L. A Model for Orientational Diffusion in Fiber Suspensions *Phys. Fluids* **7(8)**:2086–2088, 1995.
16. Rahnama, M., Koch, D.L. & Shaqfeh, E.S.G. The Effect of Hydrodynamic Interactions on the Orientation Distribution in a Fiber Suspension Subject to Simple Shear Flow *Phys. Fluids* **7**:487–506, 1995.
17. Olson, J.A., & Kerekes, R.J. The motion of fibers in turbulent flow *J. Fluid Mech.* **19**:47–64, 1998.

18. Parsheh, M., Brown, M.L. & Aidun, C.K. On the Orientation of Stiff Fibers Suspended in a Turbulent Flow in a Planar Contraction *J. Fluid Mech.* **545**:245–269, 2005.
19. Hyensjo, M. & Dahlkild, A. Study of the rotational diffusivity coefficient of fibers in planar contracting flows with varying turbulence levels *Int. J. Multiphase Flow* **34**:894–903, 2008.
20. Phan-Thien, N., Fan, X.J., Tanner, R.I., Zheng, R. FolgarTucker constant for a Fiber Suspension in a Newtonian Fluid *J.Non-Newt. Fluid Mech.* **103**:251–260, 2002.
21. Rahnama, M., Koch, D.L., Iso, Y. & Cohen, C. Hydrodynamic, Translational Diffusion in Fiber Suspensions Subject to Simple Shear-Flow *Phys. Fluids A* **5**:849–862, 1993.
22. Leal, L.G. & Hinch, E.J. The Effect of Weak Brownian Rotations on Particles in Shear Flow *Chem. Eng. Comm.* **108**:381–401, 1971.
23. Lin, J. & Zhang, L. Numerical Simulation of Orientation Distribution Function of Cylindrical Particle Suspensions *App. Math. Mech.* **23**:906–912, 2002.
24. Parsheh, M., Brown, M.L. & Aidun, C.K. Variation of Fiber Orientation in Turbulent Flow Inside a Planar Contraction with Different Shapes *Int. J. Multiphase Flow* **32**:1354–1369, 2006.
25. Stover, C.A., & Cohen, C. The Motion of Rodlike Particles in the Pressure-Driven Flow Between Two Flat Plates *Rheologica Acta* **29**:192–203, 1990.
26. Moses, K.B., Advani, G.S., & Reinhardt, A. Investigation of fiber motion near solid boundaries in simple shear flow *Rheologica Acta* **40**:296–306, 2001.
27. Magda, J.J., Tirrell, M., & Davis, H.T. The Transport Properties of Rod-like Particles. II. Narrow Slit Pore *J. Chem. Phys.* **88**:1207–1214, 1988.
28. Olson, J.A., The effect of Fiber Length on Passage Through Narrow Apertures *Doctoral Thesis, University of British Columbia* Vancouver, Canada, 1996.
29. Nitsche L.C., & Hinch E.J. Shear-induced lateral migration of Brownian rigid rods in parabolic channel flow *J. Fluid Mech.* **232**:1–21, 1997.
30. Schiek R.L., & Shaqfeh E.S.G. Cross-streamline migration of slender Brownian fibres in plane poiseuille flow *J. Fluid Mech.* **332**:23–39, 1997.
31. Doi, M. & Edwards, S.F. The theory of polymer dynamics *Oxford University Press* New York, 1984.
32. Krochak, P.J., Martinez, D.M., & Olson, J.A. The Orientation of Semi-Dilute Rigid Fiber Suspensions in a Linearly Contracting Channel *Phys. Fluids* **20**, DOI: 10.1063/1.2949277, 2008.
33. Rahnama, M., Koch, D.L. & Cohen, C. Observations of Fiber Orientation in Suspensions Subject to Planar Extensional Flows *Phys. Fluids* **7**:1811–1817, 1995.
34. Stover, C.A., Koch D.L. & Cohen, C. Observation of Fiber Orientations in Simple Shear Flow of Semi Dilute Suspensions *J. Fluid Mech.* **238**:277–296, 1992.
35. Martinez, D.M., Buckley, K., Jivan, S., Lindström, A., Thurigaswamy, R., Ruth, T.J. & Kerekes, R.J. Characterizing the mobility of fibers during sedimentation *Pulp Pap. Fund. Res. Symp. (Oxford)*, **1**:225–254, 2001.
36. Xu, H.J., & Aidun, C.K. 2005 Characteristics of Fiber Suspension Flow in a Rectangular Channel *Int. J. Multiphase Flow* **31**, 318–386.

Transcription of Discussion

NEAR-WALL ESTIMATES OF THE CONCENTRATION AND ORIENTATION DISTRIBUTION OF SEMI-DILUTE RIGID FIBER SUSPENSIONS IN POISEUILLE FLOW

Paul J. Krochak,[1] *James A. Olson*[1] and *D. Mark Martinez*[2]

[1]The Pulp and Paper Center, Dept. of Mechanical Engineering, The University of British Columbia, 2324 Main Mall, Vancouver BC, V6T 1Z4, Canada
[2]Dept. of Chemical and Biological Engineering, The University of British Columbia, 2360 East Mall, Vancouver, BC, V6T 1Z3, Canada

Jari Hämäläinen University of Kuopio

You mentioned flocculation as a future development. What kind of plans do you have for modelling of flocculation?

Paul Krochak

Loosely speaking, we are working on including shear-induced migration into our models. We are going to separate the equations for the concentration and orientation distributions. This can be shown to be possible with a little bit of math, however these separated equations are not actually decoupled. This provides a model for the concentration variation independent from the orientation equations. The general solution scheme is to first solve the concentration equations, which is then used in the orientation equations which are then

solved. So now we'll have a concentration which is somewhat decoupled from orientation – the orientation however is strongly coupled to concentration across the entire channel.

Jean-Claude Roux University of Grenoble

In your experiments, you have done trials on a channel where the section area is rectangular. That is why your hypothesis of orientation distribution in the plane and the results you show are in agreement. What do you think about the extension to a circular section?

Paul Krochak

As in a pipe?

Jean-Claude Roux

Yes, as in a pipe, for example.

Paul Krochak

Well, I think along the central axis, when you chop the pipe in half, it would probably look quite similar. Of course, you would have to express yourself mathematically in cylindrical coordinates opposed to rectangular ones, but I think they would be quite comparable. I suppose it may not be so trivial to answer that question, in regions of curvature, but I think that the results would carry over quite nicely. Just off the top of my head, I think that it might actually compare better since fibres can be located in the corner of a rectangular channel and freely rotate out of plane, where if there's curvature in this location, the fibre will have less volume in which it can freely rotate. It's possible the results might actually compare better.

Jean-Claude Roux

Okay, and I have another question that is probably more simple. In figure eight when you represent the orientation anisotropy, you have some oscillations. Have you an understanding of these oscillations of the orientation anisotropy profile?

Paul Krochak

So again, these oscillations are something that we're seeing everywhere and really the peak to peak is approximately one fibre length. So we think that these fibres are interacting hydrodynamically and that fibres are segregating into small flocs. Perhaps this is a phenomenon caused by hydrodynamic interactions? Specifically I think it is shear-induced migration.

Daniel Söderberg Innventia / KTH

Two questions: the first is did you measure what you call the out-of-plane orientation? Have you made an attempt from the visualizations you have to get that?

Paul Krochak

Yes, we have measured out of plane orientation. I can say the real reason why we have kept to this in-plane analysis is that the system becomes numerically much more difficult to solve, at least from a time perspective. So to implement these boundary conditions on two walls takes quite a bit of time, almost more so than I have patience for. But for the few results that we did predict, the magnitude of the plots I have shown reduces considerably so that we'd probably get much better agreement with the experiments. I have not actually compared this case, but the one clear trend, if you go to 3D calculations of fiber orientation, is that these plots always reduce in magnitude, so you would get much better agreement with the experiments. The other clear finding is that when fibres come near a wall, the out-of-plane orientation becomes extremely random, so it is almost the exact opposite of what we see with the in-plane analysis near the walls. The out-of-plane orientation near the point $y = 0$, or the lower wall, becomes almost fully isotropic. This is what we have predicted. I cannot say that I have really analyzed this case experimentally.

Daniel Söderberg

Well, I think we have seen that you can get clearly anisotropic distributions close to solid walls. So they're all flowing perpendicular to the flow direction, which is a little bit amazing. But you have the data to get out-of-plane, since you have the length of the fibre?

Discussion

Paul Krochak

Yes. We had originally started doing that but the one thing we wanted to focus on here is on the near wall and the x, y plane or at least in one plane. So to split the image of the camera (as we had done) took away half the resolution. We collected a bunch of data in this manner and then went back and said "let's try and get a little better accuracy near the wall". So we did another set of data where the entire lens looked at just the x, y planes, we did not split the image to see the top and the front. Two cameras would probably help.

Daniel Söderberg

Yes, and you have the length of the fibres which could give some sort of an estimate.

Paul Krochak

Yes, that is true.

Daniel Söderberg

But if you consider the oscillations. Did you try to take the cameras and, instead of imaging the whole channel which I guess you did, did you just image a very small region with very high resolution to see if you can get a better peak resolution, and also see the oscillations in that?

Paul Krochak

Yes, that is a good idea; we did not do that, but that is a good idea

Tetsu Uesaka FPInnovations

How did you determine D_t or D_r (the translational and rotational diffusion coefficients) in the experiments? It seems to be space-dependent in your case.

Paul Krochak

Yes, I did fail to mention that, so let's just remind everyone what we're talking about here. Looking at the orientation equations, D_t models the effect of the

fibre–fibre hydrodynamic interactions on the orientation of the fibre. So D_t essentially says that where these fibres interact, they create a randomization effect, it's a rotational diffusion coefficient. As for D_t, we essentially ballparked it, we kept it constant, we looked it up a little bit in the literature, we got some sort of theoretical order of magnitude for it. Actually, it was quite small, about 10^{-4}. Both are actually quite small. D_r, we actually used what's referred to as a Folder-Tucker estimate for it – it just essentially scales with the local strain rate. We have measured D_r in our previous study and then D_t as I said we really kind of ballparked it.

Bill Sampson University of Manchester

You talked a fair bit about, or you've alluded to, the effects of flocculation of fibre interaction, and your nL^3 values are about 11 and 3.6 which is say about double the crowding numbers. So these are really very dilute suspensions, with quite low flocculation propensities. Did you make any measurements of higher consistency suspensions?

Paul Krochak

We did actually. We have gone up to nL^3 equals about 20.

Bill Sampson

Okay, that is a crowding number of about 10 so it's still in a very a soft-flocced type regime.

Paul Krochak

Yes, and again the results turned out to be quite similar to $nL^3 = 10$.

Bill Sampson

Which isn't really that surprising is it, because you've not really started to get into the regime where these interactions are really going to matter.

Paul Krochak

Right, but bear in mind, the difference is that it is such a low Reynolds number flow. In a high Reynolds number flow, the turbulence will start to damp out these interactions, and the turbulent fluctuations will just

completely outweigh these hydrodynamic interactions. But at this lower Reynolds number, I think this is why we are seeing more oscillations and things which we feel are really due to flocculation; the flow is so slow, the fibres can really feel each other.